

## COASTAL TURBIDITY MONITORING USING THE PROBA-V SATELLITE

Els Knaeps<sup>1</sup>, Sindy Sterckx<sup>1</sup>, Nitin Bhatia<sup>2</sup>, Qilong Bi<sup>3</sup>, Jaak Monbaliu<sup>3</sup>, Erik Toorman<sup>3</sup>, André Cattrijse<sup>4</sup>, Liesbeth De Keukelaere<sup>1</sup>

### Abstract

Proba-V is a Belgian satellite designed for global vegetation monitoring. Because of its good image quality and the coverage of coastal waters, there are opportunities to expand its use to other applications. Here Proba-V is used to derive turbidity of coastal waters. A complete new processing chain was developed including algorithms for cloud masking, atmospheric correction and turbidity retrieval. The processor was used to derive turbidity products for the North Sea in 2015-2016. Validation of the products was performed using Aeronet-OC stations (validation of the reflectance) and CEFAS smartbuoys (validation of the turbidity). In addition a comparison is ongoing between the turbidity derived from the remote sensing and a model developed for the North Sea area set up using the TELEMAC-MASCARET model suite.

**Key words:** Proba-V, remote sensing, turbidity, satellite, model

### 1. Introduction

Satellite observations are a valuable source of information for coastal managers. The area covering information and historic dataset can significantly add information to data obtained from field observations and outcome from models. The most widely used parameters derived from remote sensing are the Turbidity (T) and Suspended Particulate Matter (SPM) concentrations of the surface waters. Surface water refers to the upper meters, exact penetration depths depending on the turbidity of the water column. Both parameters can be derived from the satellite imagery because there is a clear relationship with the water reflectance collected by the satellite sensor. Turbidity, as optical property, is more directly related to the water reflectance and the relationship is therefore less influenced by changing particle size and composition (Dogliotti et al., 2015). Both parameters are traditionally derived from a set of Ocean Colour (OC) sensors with spatial resolution of 0.25-1km and a revisit time of 1 day. Examples include the Moderate resolution imaging spectrometer (MODIS) (Wang et al., 2012; Miller and McKee, 2004), the Medium Resolution Imaging Spectrometer (MERIS) (Loisel et al., 2014; Gohin, 2011) and its successor Sentinel-3. However each single OC sensor has a limited spatial coverage of the coast and provides limited information on TSM/T dynamics in near shore areas. Therefore the OC community has already been looking to some extent to non-OC sensors, i.e. sensors designed for other purposes such as atmosphere or vegetation monitoring. It is recognized that their performance (e.g. Signal to Noise Ratio) is less than the OC sensors but at least for TSM/T they provide a wealth of new information. Examples include Landsat (Montanher et al., 2014; Vanhellemont and Ruddick, 2014), SEVIRI (Vanhellemont et al., 2014), Deimos (Caballero et al., 2014) and Formosat (Miller et al., 2011).

Proba-V is a Belgian satellite and good example of a non-OC sensor designed for vegetation monitoring with daily coverage at 300 m and a 5-daily coverage at 100m spatial resolution. The sensor onboard the satellite records data up to at least 100 km away from the coastlines. Although the sensor has very broad spectral bands, the good image quality provides opportunities for turbidity retrieval in coastal waters. Combining turbidity products from Proba-V and other typical OC sensors allows for better monitoring of turbidity in dynamic near shore areas and it increases the chance to detect short term events in particular for areas with rapid changing cloud cover. The study aims to demonstrate the added value of Proba-V for coastal turbidity monitoring, thereby opening the way for the exploitation of future broadband sensors for the same purpose.

The objective of the paper is to derive turbidity from the Proba-V satellite products. As no software was

available for the processing of Proba-V data for water surfaces, a dedicated processing chain is developed including an atmospheric correction algorithm and turbidity algorithm. The accuracy of the retrieved products is assessed through a direct validation with field water reflectance and field turbidity data. Finally, as an application, we demonstrate how the derived turbidity maps can be used to improve the functioning of sediment transport models.

## 2. Study area

The main test site is located within the Southern North Sea: the Belgian coastal zone, Western Scheldt and the English Channel. Within the study area there are several stations/buoys which deliver data for validation of the Proba-V products (Smartbuoys, Aeronet-OC indicated in Figure 1).



Figure 1: study area

## 3. Proba-V processing chain

Several processing steps are needed to derive a turbidity product from a raw Proba-V image. These include masking of non-water pixels and masking of pixels contaminated with sun glint and white caps. Then the water pixels are corrected for atmospheric artifacts, i.e. absorption and scattering by atmospheric constituents to obtain water reflectance product i.e. solar radiation reflected from the water surface that carries information on its constituents. This water reflectance can then be related to the turbidity to generate a 2D turbidity map. The different steps are elaborated below.

## 4. Land and cloud masking

The raw Proba-V images are delivered as Top-Of-Atmosphere reflectance, i.e. reflectance not corrected for any atmospheric effects. On these images a first land and cloud masking is applied based on simple thresholds of the PROBA-V Short Wave InfraRed (SWIR) band, centered around 1665 nm. In the SWIR wavelength range (1000 – 3000 nm) the water reflectance is very distinct from the land and cloud reflectance as the pure water absorption is very high (Figure 2) resulting in an extremely low water reflectance (Knaeps et al., 2015). Beyond 1300nm we can assume zero reflectance from the water and the image will appear very dark over water surfaces. In turn, the cloud reflectance in the SWIR is very high.

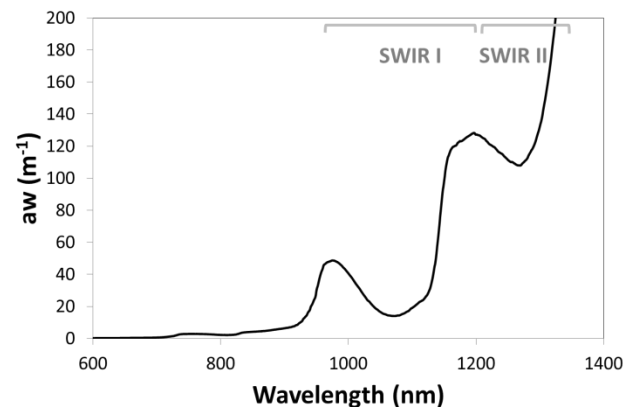


Figure 2: Pure water absorption ( $a_w$ )

## 5. Sun glint masking

Pixels in the Proba-V image affected by sun glint, i.e. the direct reflection of the sunlight into the sensor field-of-view, are masked. For a flat sea surface (zero wind speed) the specular reflectance or directly reflected light can be computed ‘exactly’ using the Snell-Fresnel laws. For a rough sea surface, the reflection is conditioned by the wind and therefore the sun glint reflectance of the sea surface can only be described on statistical basis in function of wind speed. The Cox-Munk (Cox and Munk, 1954) formalism is commonly used to calculate the wind speed-wave slope distribution. Here, we adapted the isotropic Gaussian slope distribution (isotropic rough surface, independent of wind-direction) to represent the oceanic wave slopes. These isotropic wave slope Probability Distribution Function (PDF) is often used in remote sensing applications when wind direction is not accurately known or not uniform.

## 6. White caps masking

White caps are generated by breaking waves. The sea surface might be largely contaminated by these whitecaps especially for high wind speeds. In case wind speed information is available pixels or images contaminated by surface white caps can be discarded based on a wind speed threshold (10 m/s). For wind speeds lower than 10 m/s the whitecaps reflectance is small and can therefore be neglected.

## 7. Atmospheric correction

In the presence of Earth’s atmosphere, the reflectance received at the sensor differs from the target reflectance. This is primarily because of the complex interaction of the surface reflected radiation with the atmospheric constituents while propagating along the path from the target surface to the sensor. The interaction generates two main atmospheric effects: absorption by atmospheric gases and aerosols and scattering by aerosols and molecules. In addition, on the path of the beam to the sensor two major scattering components distort the at-sensor radiance: reflection by the surrounding area of the target pixel and radiance backscattered by the atmosphere that did not interact with the surface. An Atmospheric Correction algorithm is applied to retrieve the radiance reflected at the surface from the at-sensor radiance which in turn is used to derive useful information on the water constituents. This is done by modeling the scattering and absorption properties of the atmosphere with radiative transfer codes based on solar and viewing angles, atmospheric pressure, the Aerosol Optical Thickness (AOT) and the aerosol model.

### 2.1. Aerosol retrieval

The main challenging components of the atmospheric correction are the retrieval of the AOT and aerosol type at the time of imaging. Taking into account the specifications of PROBA-V, we consider two methods: 1) based on spatial extension of aerosol information retrieved from nearby land (Guanter *et al.*, 2007; Guanter *et al.*, 2010) and 2) based on extending the “black pixel” approach to the SWIR. The SWIR black pixel approach assumes that the contribution of in-water constituents is zero due to the high absorption of pure water in the SWIR. The signal in the SWIR can thus be assumed to be entirely atmospheric and can therefore be employed for the aerosol determination.

The final A/C approach can be a “merging” of both methods e.g. for nearshore pixels a land-based approach is used, while for offshore pixels the NIR-SWIR approach is preferred. In this paper, only the results for the land based approach are discussed.

## 2.2. Radiative transfer simulations

Once the AOT (and aerosol type) is known the actual atmospheric correction parameter are calculated by a multi-parameter LUT interpolation. The Moderate-Resolution Atmospheric Radiance and Transmittance Model-5 “MODTRAN5” (Berk *et al.*, 2006) is used for the radiative transfer calculation. A look-up table is calculated to speed up the correction procedure.

## 8. Turbidity retrieval

The one-band algorithm developed by Nechad *et al.* (2009) is selected to derive turbidity from the Proba-V water reflectance. The algorithm relates turbidity (T, in FNU) to the water reflectance  $\rho_w$  through,

$$T = \frac{A_T^{\rho} \cdot \rho_w(\lambda)}{\left(1 - \frac{\rho_w(\lambda)}{C_T^{\rho}}\right)}, \quad (1)$$

where  $A_T^{\rho}$  and  $C_T^{\rho}$  are wavelength dependent calibration coefficients.

$C_T^{\rho}$  is calculated using standard inherent optical properties. The  $A_T^{\rho}$  coefficient was obtained by a non-linear regression analysis using in situ measurements of T and  $\rho_w$ . The  $A_T^{\rho}$  is tabulated for every 2.5 nm in Nechad *et al.* (2009). This coefficient is later improved in Dogliotti *et al.* (2011) (only for MODIS bands) based on an extended set of in-situ data. Here the  $A^{\rho}$  and  $C^{\rho}$  parameters are resampled for the PROBA-V RED and NIR bands (Table 1). For the resampling of  $A_T^{\rho}$  (NIR) the tabulated values in Nechad *et al.* (2009) are spectrally resampled and the retrieved value is adjusted considering the percentage change proposed by Dogliotti *et al.* (2011) with respect to the Nechad *et al.* (2009) values.

Table 1. Resampled calibration coefficients  $A_T^{\rho}$  and  $C_T^{\rho}$  used to retrieve T for the PROBA-V RED and NIR bands

PROBA-V band	$A_T^{\rho}$ (resampled)	$C_T^{\rho}$ (resampled)
RED (583 – 732 nm)	237.891	0.168
NIR (743 – 942 nm)	2535.41	0.209

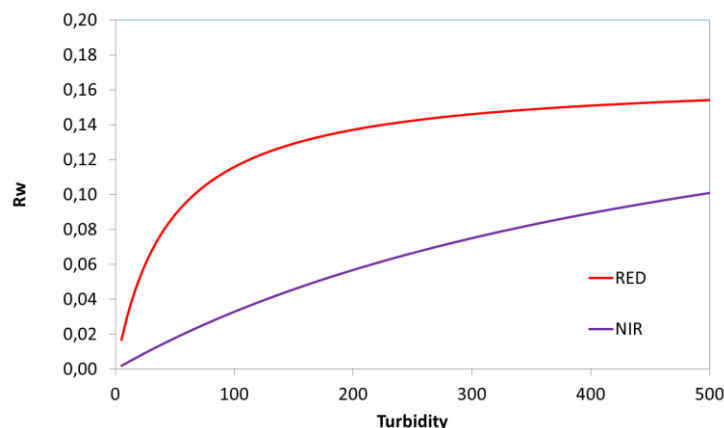


Figure 3. PROBA-V water leaving reflectance in RED and NIR bands as a function of the turbidity, following the Nechad *et al.* (2009) algorithm

The reflectance in the RED band is very sensitive to low (0 – 50 FNU) and medium (50 – 100 FNU) turbidity where the relationship is approximately linear. At higher turbidity (> 100 FNU), however, the

relationship tends to saturate. While the NIR is less sensitive to low—medium turbidity, saturation seems to occur only at very high turbidity. Because sensitivity of water-leaving reflectance to turbidity is a function of wavelength, a so called wavelength switching based turbidity retrieval algorithms has been proposed by various authors (e.g. Han et al., 2016, Shen et al. , 2010; Dogliotti et al. , 2015).

Also here a switching is proposed between Red and NIR spectral bands. This switching approach is generally preferred for coastal waters with large variations in turbidity values. The Red- to NIR switching values (i.e. at which turbidity levels switching is performed between Red and NR wavelengths) were selected based on the saturation of the most sensitive bands as proposed by Novoa et al. (2017).

For turbidity values between 0 and 2000 FNU the Proba-V Red and NIR band reflectance was estimated according to equation [1]. The Red band was regressed against the NIR band and a logarithmic regression curve was modeled through the data points as shown in Figure-4. The saturation of the most sensitive band starts where the slope of the tangent line is 1. This corresponds to  $\rho_w(RED)=0,1$  which corresponds to a turbidity of 60 FNU.

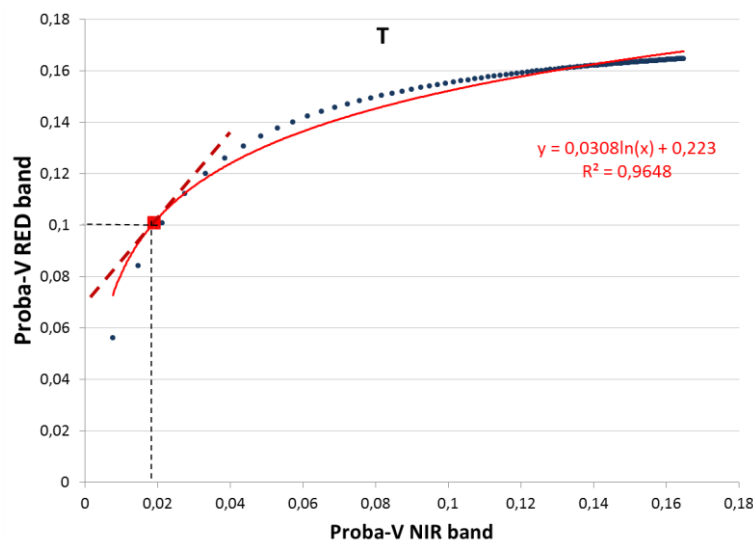


Figure 4. Relationship between PROBA-V RED and NIR reflectance

To obtain smooth transitions in the processed T images a switching window is proposed between  $\rho_w(RED)=0,09$  and  $\rho_w(RED)=0,11$ . These windows correspond to T values of 46 and 76 FNU.

In summary:

- For  $\rho_w(RED) < 0,09$  use T derived on the basis of the RED band
- For  $\rho_w(RED) > 0,11$  use T derived on the basis of the NIR band
- For  $0,09 < \rho_w(RED) < 0,11$  perform merging :

$$T = (1-w) * T(RED) + w * T(NIR)$$

Where w changes linearly from 0 at  $\rho_w(RED)=0,09$  to 1 at  $\rho_w(RED)=0,11$ .

## 9. Validation

### 2.3. Field data for direct validation

Proba-V water reflectance is validated using data available from the Aerosol Robotic Network (AERONET)—Ocean Color (AERONET-OC) sites. AERONET is developed to sustain atmospheric studies at various scales with measurements from worldwide distributed autonomous sun-photometers. The AERONET network has been extended to support marine applications. This new network component is

called AERONET-OC. AERONET-OC provides the additional capability of measuring the water leaving radiance emerging from the sea.

Aeronet-OC station data is obtained from the Aeronet website (<http://aeronet.gsfc.nasa.gov/>). Two sites are used in the validation exercise:

Table 1: AERONET-OC stations used for validation

Station name	coordinates
Thornton_C-power	51°31'57"N 02°57'19"E
Zeebrugge-MOW1	51°21'43"N 03°07'12"E

As can be seen in Figure 5, PROBA-V spectral bands are much broader than the AERONET-OC spectral bands, which complicates the “direct” comparison. In order to take into account the difference in center wavelength and band width “a spectral shift” correction is applied before performing the “direct” comparison.

To determine the spectral shift correction coefficients, hyperspectral in-situ measured  $\rho_w$  spectra acquired from the Scheldt, La Plata and Gironde estuary in the frame of the SeaSWIR project (Knaeps et al., 2015) and  $\rho_w$  spectra from the North Sea from the Coastcolour dataset (Nechad et al., 2015) are used.

These in-situ datasets are spectrally resampled to both the PROBA-V and the AERONET-OC spectral bands. Next, a regression analysis is performed between the resampled  $\rho_w$  data for the corresponding bands to determine the “spectral shift” coefficient to be applied to the real data. Note, that for the blue band this spectral correction function will consider the two AERONET-OC bands to incorporate both edges of the PROBA-V blue band.

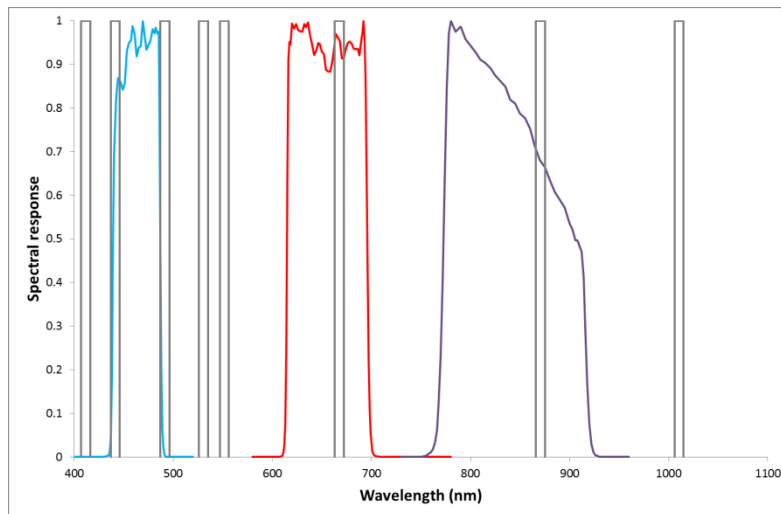


Figure 5: Comparison of spectral response of AERONET-OC (in grey) and PROBA-V spectral bands.

Proba-V turbidity is validated using the CEFAS SmartBuoys. These autonomous systems are moored, automated, multi-parameter recording platforms used to collect marine environmental data. Turbidity data are typically collected every 30 minutes at 1m water depth. The data are freely available for research purposes. In the North Sea study area there are three Buoys currently in operation. These are: 1) Warp (TH1) NMMP in the turbid waters of the Thames; 2) West Gabbard and 3) Dowsing located more offshore. One more buoy outside the study area is used: the Liverpool Bay Coastal Observatory.

Table 2: Smartbuoy stations used for validation

Station name	coordinates
Warp (TH1) NMMP	51.52633°N 1.028167°E

West Gabbard	51.98033°N 2.082833°E
Dowsing	53.53133° N 1.056°E
Liverpool Bay	53.5345°N 3.361833°W

#### 2.4. Validation procedure

Test datasets were created consisting of cloud-free PROBA-V data in the period 2015-2016 and reference data from AERONET CIMEL instruments and Smartbuoys .

For each PROBA-V overpass (over the test site) the water leaving reflectance and turbidity of a nominal pixel containing the location of the field data measurement was extracted. The threshold for the temporal offset between the time of the PROBA-V overpass and field data measurement was set as  $\pm 1$  hour.

### 10. Results

In Figure 6 the spectral shift correction functions for Aeronet-OC based on the SeaSWIR dataset are given. Each region (La Plata, Gironde, Scheldt) is shown in a different colour. The one-to-one line is shown in red. For the PROBA-V BLUE and RED band a single, site independent, spectral shift correction function can be found with a  $R^2$  better than 0.99. For the NIR band some variability seems to exist between sites.

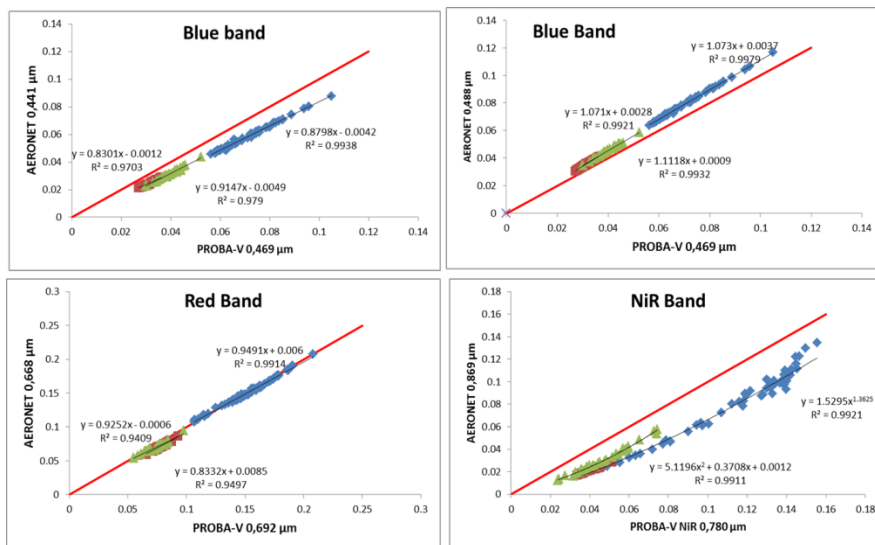


Figure 6 Spectral shift functions using the SeaSWIR dataset – Red: La Plata, green: Scheldt, blue: Gironde. Red line is the one-to-one line

Figure 7 shows the validation results from the Thornton and Zeebrugge Aeronet-OC stations for the Proba-V water reflectance in the blue, Red and NIR band. The Proba-V reflectances are converted using the coefficients from Figure 6. Correlations for the two blue bands are good ( $R^2$  is 0.67 and 0.69) with a small slope difference with respect to the one-one line. The Red band has a high correlation ( $R^2 = 0.72$ ) but a small bias is observed. For the NIR band there was no correlation found between the Aeronet OC water reflectance and the Proba-V water reflectance. This suggests that the Proba-V NIR band cannot be used to derive turbidity in low to moderately turbid waters and additional validation is needed in highly turbid waters.

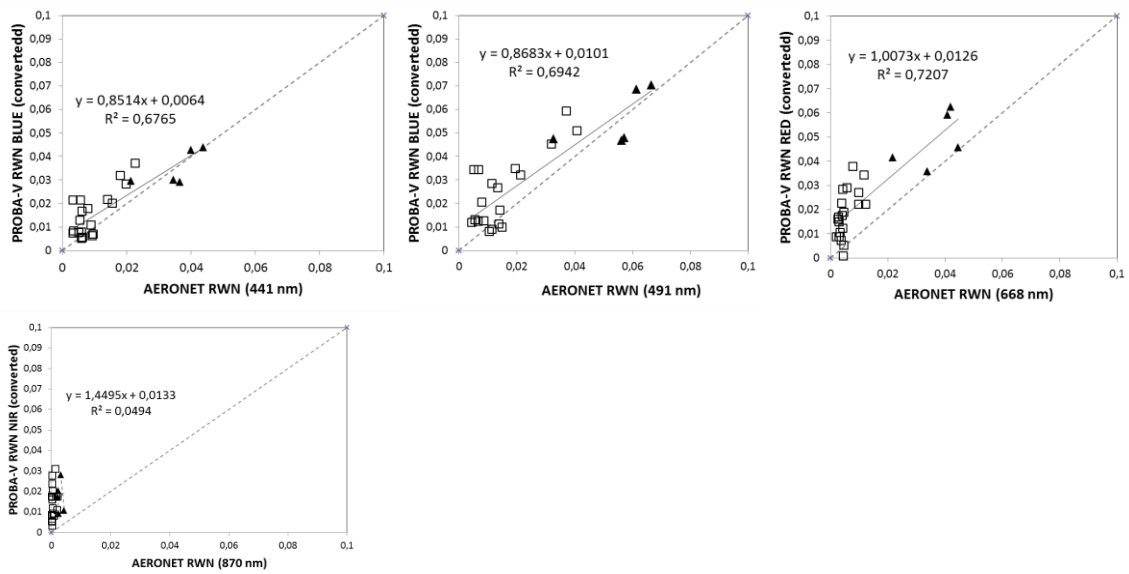
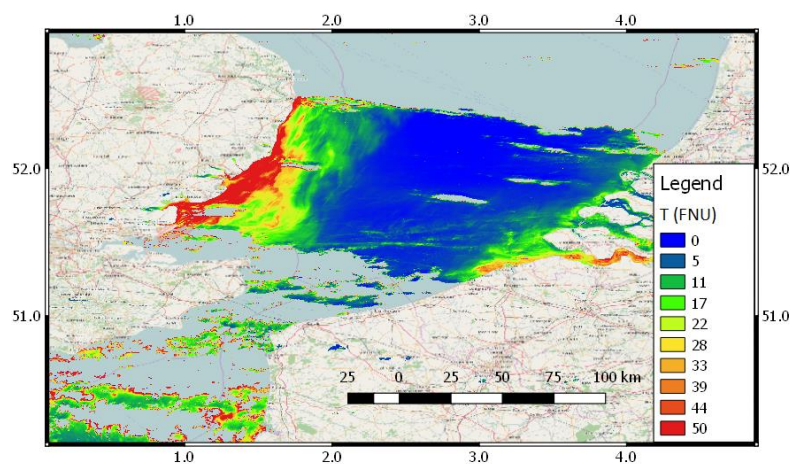


Figure 7: Regression plots of the water reflectance from in situ and water reflectance from Proba-V for three different wavelengths (left: 441 nm, middle: 491 nm and right: 668 nm; bottom: 870nm). The square are results from the Thornton Aeronet-OC station, the triangles are results from the Zeebrugge MOW Aeronet-OC station.

Three turbidity maps are shown in Figure 8 for April 2015 (16, 20 and 21 April). Only the results for the central Proba-V camera are shown which provides the highest spatial resolution (100m). Clouds were present in the images, particularly on the 16<sup>th</sup> of April. The Proba-V processor was able to detect and mask these clouds fairly well. The pixels covered with clouds are blank and not further processed. Some artifacts are present in the first image where pixels at the boundary of the clouds are not masked and show higher turbidity values than the surroundings. This can be due to adjacency effects of the nearby clouds through scattering in the atmosphere. This adjacency effect results in higher reflectance values of the target pixel and hence higher turbidity values. On 20 and 21 April some contrails produced by airplanes are visible in the images and not masked.

The observed turbidity values and patterns are realistic with lowest values in the central part of the North Sea and high turbidity introduced by the Thames river in the West and the Scheldt river in the East.





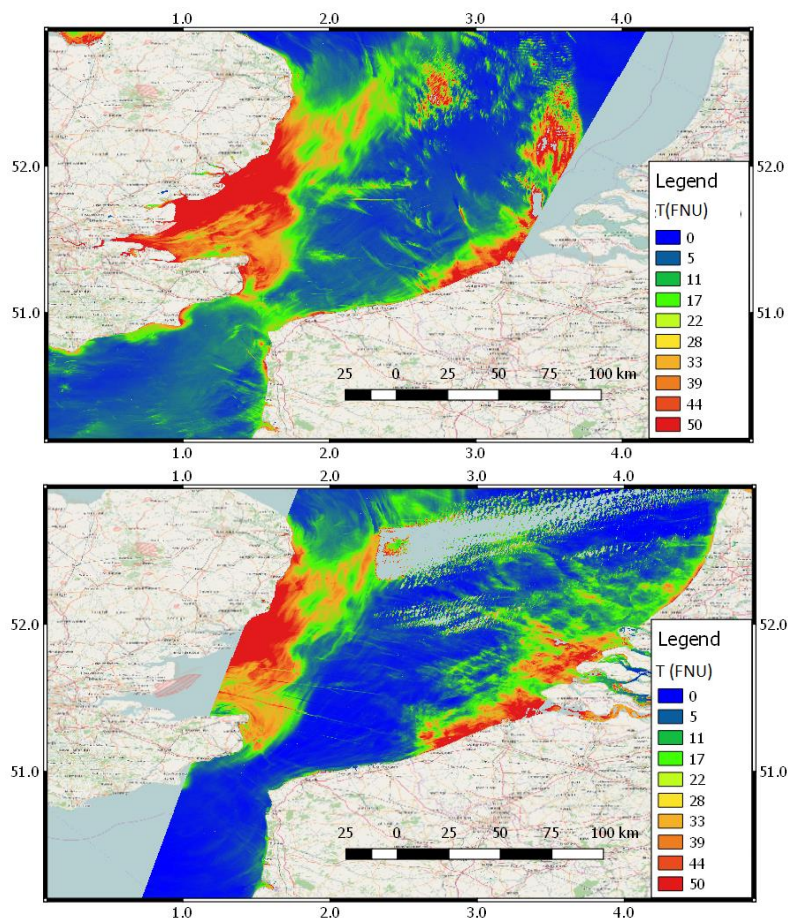
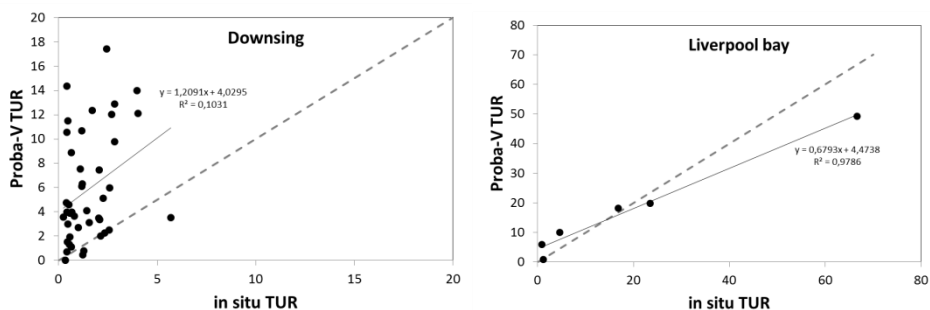


Figure 8: Turbidity maps from Proba-V for the North Sea: Top) 16 April 2015, Middle) 20 April 2015 and bottom) 21 April 2015

The validation results using the turbidity from the CEFAS smartbuoys are shown in Figure 9. The best results are obtained for stations Liverpool bay and Warp. Liverpool bay has a high correlation coefficient but a slope difference can be observed with the on-one line in grey. In the Warp station an offset can be observed. The offset might be due to the atmospheric correction (offset already observed in the Rw validation in Figure 7) but the slope difference might have other reasons (see further in discussion). For station Downsing Proba-V overestimates the turbidity. This can be due to the overall low turbidity levels at this station (max value of 5 FNU measured in situ). The Proba-V SNR might be insufficient to derive quality estimated for these low turbidity areas.



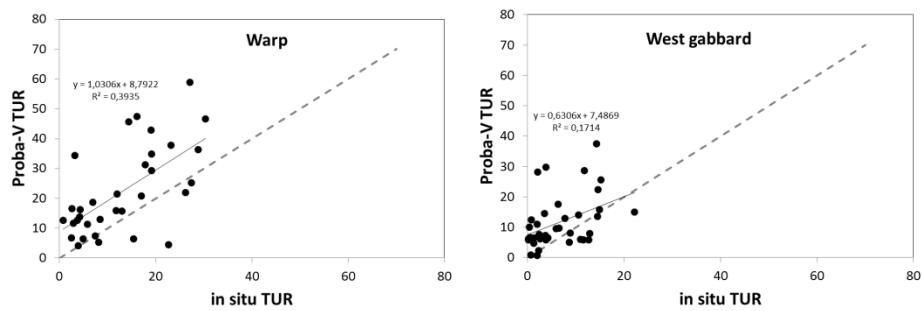


Figure 9: regression plots between in situ and Proba-V turbidity for all the smartbuoy locations

## 11. Comparison with calculated concentration from hydrodynamic and sediment transport modelling

A model for the North Sea area has been set up using the TELEMAC-MASCARET model suite consisting of a hydrodynamic module (TELEMAC), a wave module (TOMAWAC) and a sediment transport module (<http://www.opentelemac.org/>). The sediment module can estimate sediment concentrations which can be compared to the SPM/turbidity values estimated from RS-images. The model is based on finite elements easily allowing for flexible mesh sizes of the computational grid near the coast, see figure 10 below.

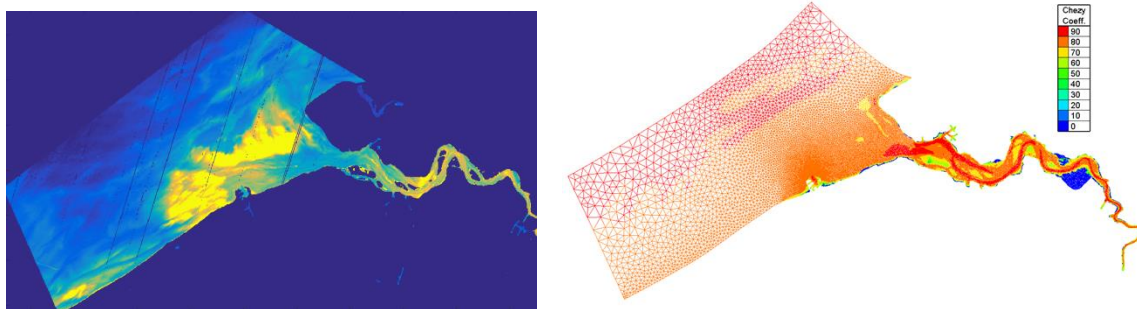


Figure 10: Left: PROBA-V image cropped to the modelling domain, of which the mesh and roughness map (cf. Bi & Toorman, 2015) is shown on the right.

The model can be run in 2D or 3D. The 3D approach makes it possible to assess the variation of the concentration over the vertical. Different model set-ups will be used to assess the importance of e.g. flocculation formulations (Bi et al., 2016) in the sediment transport module. The intercomparison of the RS obtained SPM/turbidity with the model calculated SPM/turbidity is not an easy task. Three approaches will be used to quantify the error signal. A first approach is an Euclidian distance approach which can be applied to a predefined subdomain and for a particular length scale. A second approach is based on structure similarity expressed by the Structure Similarity Index (SSIM) developed by Wang et al. (2004) which eliminates some of the drawbacks of the pointwise signal differences in the distance based approach by taking into account the underlying signal structure. A third approach searches for local pattern shifts. It is a pattern recognition approach based on cross-correlation of two signals which are displaced one relative to the other. Further details are discussed in Qilong et al. (2017).

## 12. Discussion

When comparing turbidity products from remote sensing and in situ, it is important to understand how the turbidity is measured and how the turbidity algorithm is developed. Differences in the turbidity values between the smartbuoys and the Proba-V turbidity product can partly be attributed to the different turbidity

meters used. The Smartbuoys are equipped with a Seapoint turbidity meter with operating wavelength at 880 nm and recording light scattered by suspended particles between 15° and 150°. The Nechad (2009) algorithm is developed based on measurements with a HACH portable turbidity meter with operating wavelength at 860 nm and recording side scattering at 90°. Despite the fact that they are both calibrated with standard Formazine suspensions, their response in natural waters might differ (Roesler & Boss, 2008) because of the intrinsic difference in measurement method. Slope differences as observed in Figure 9 might be attributed to these differences in measurement principle.

Next to the turbidity products developed here from Proba-V, also a SPM product can be derived. It can be derived using a regional SPM-T relationship developed to convert the turbidity values to corresponding SPM concentrations. The best way to establish such relationship is based upon in-situ turbidity measurements performed using a similar turbidity meter as used by Dogliotti et al. (2015) and Nechad et al. (2009).

Future work includes a global validation using Aeronet-OC stations out of the study area, the incorporation of the SWIR AOT retrieval to further improve the quality of the results and finally an intercomparison with MODIS turbidity products.

### Acknowledgements

The research leading to these results has received funding from the Belgian Science Policy Office through the STEREO programme (Proba4Coast project) and the European Space Agency through the PV-LAC project.

We thank CEFAS for making available the smartbuoy data (<https://www.cefas.co.uk/cefas-data-hub/smartbuoys/>)

### References

- Berk, A., G.P. Anderson, P.K. Acharya, L.S. Bernstein, L. Muratov, J. Lee, M. Fox, S.M. Adler-Golden, J.H. Chetwynd, M.L. Hoke, R.B. Lockwood, J.A. Gardner, T.W. Cooley, C.C. Borel, P.E. Lewis and E.P. Shettle, "MODTRAN5: 2006 Update," *Proceedings SPIE*, Vol. 6233, 62331F, 2006
- Bi, Q., Toorman E.A. 2015. Mixed-sediment transport modelling in the Scheldt estuary with a physics based bottom friction law. *Ocean Dynamics*, 65:555-587.
- Bi Q, Ernst S, Lee B, Toorman E. 2016. Implementation of two-class population balance equation bimodal flocculation model in TELEMAC-3D. *TELEMAC-MASCARET User Conference*. (Oct.2016, Paris, FR), pp. 11-13.
- Bi, Q., J Royakkers, N. Bhatia, S. Sterckx, E. Knaeps, E. Toorman and J. Monbaliu, 2017. Validation of satellite remote sensing for coastal turbidity monitoring by sediment transport modelling. *INTERCOH*, Montivideo, 2017.
- Caballero, I., Morris, E.P., Ruiz, K., Navarro, G. 2014. Assessment of suspended solids in the Guadalquivir estuary using new DEIMOS-1 medium spatial resolution imagery. *Remote Sensing of Environment*, 146 : 148-158
- Cox, C and Munk, W. 1954. Measurement of the roughness of the sea surface from photographs of the sun's glitter. *Journal of the optical society of America*, 44 (11): 838- 850
- Dogliotti, A.I.; Ruddick, K.; Nechad, B.; Lasta, C., 2011. Improving water reflectance retrieval from MODIS imagery in the highly turbid waters of La Plata river, in: *Proceedings of VI International Conference «Current problems in optics of natural waters» (ONW'2011)*, St. Petersburg, Russia, September 6-9, pp. 8.
- Dogliotti, A., Ruddick, K., Nechad, B., Doxaran, D., Knaeps, E. 2015. A single algorithm to retrieve turbidity from remotely-sensed data in all coastal and estuarine waters, *Remote Sensing of Environment*, 156: 157–168.
- Gohin, G. Annual cycles of chlorophyll-a, non-algal suspended particulate matter, and turbidity from space and in-situ in coastal waters, *Ocean Sci*, 7, 705-732

Guanter, LDel Carmen González-Sanpedro, M., Moreno, J., 2007. A method for the atmospheric correction of ENVISAT/MERIS data over land targets, *International Journal of Remote Sensing*, 28:3-4, 709-728.

Guanter, L., Ruiz-Verdu, A., Odermat, D., Giardino, C., Simis, S., Estelles, V., Heege, T., Dominguez-Gomez, J.-A., Moreno, J., 2010: Atmospheric correction of ENVISAT/MERIS data over inland waters: Validation for European lakes. - *Remote Sensing of Environment*, 114(3): 467—480.

Han, B.; Loisel, H.; Vantrepotte, V.; Mériaux, X.; Bryère, P.; Ouillon, S.; Dessailly, D.; Xing, Q.; Zhu, J. 2016. Development of a Semi-Analytical Algorithm for the Retrieval of Suspended Particulate Matter from Remote Sensing over Clear to Very Turbid Waters” *Remote Sensing*, 8.

Hubert Loisel and Antoine Mangin and Vincent Vantrepotte and David Dessailly and Dat Ngoc Dinh and Philippe Garnesson and Sylvain Ouillon and Jean-Pierre Lefebvre and Xavier Mériaux and Thu Minh Phan", Variability of suspended particulate matter concentration in coastal waters under the Mekong's influence from ocean color (MERIS) remote sensing over the last decade. *Remote Sensing of Environment*, 150: 218-230

Knaeps, E.; Ruddick, K.G.; Doxaran, D.; Dogliotti, A.I.; Nechad, B.; Raymaekers, D.; Sterckx, S. 2015. A SWIR based algorithm to retrieve total suspended matter in extremely turbid waters”, *Remote Sensing of Environment*, 168: 66-79.

Miller, R.L. and McKee, B.A. 2004. Using MODIS Terra 250 m imagery to map concentrations of total suspended matter in coastal areas. *Remote Sensing of Environment*, 93: 259-266

Miller, R.L., Liu, C., Buonassissi, C.J., Wu, A. 2011. A multi-sensor approach to examining the distribution of Total Suspended Matter (TSM) in the Albemarle-Pamlico estuarine system, NC, USA. 2011. *Remote Sensing*, 3 : 962-974

Montanher, O.C., Novo, E.M.L.M, Barbosa, C.C.F, Rennó, C.D. 2014. Empirical models for estimating the suspended sediment concentration in Amazonian white rivers using Landsat5/TM. *International Journal of Applied Earth Observation and Geoinformation*, 29. Pp.67-77

Nechad, B., Ruddick, K. and G. Neukermans, “Calibration and validation of a generic multisensor algorithm for mapping of turbidity in coastal waters”, in *Proceedings SPIE* Vol. 7473, 74730H., 2009.

Novoa , S., Doxaran, D., Ody, A., Vanhellemont, Q., Lafon, V., Lubac, B., Gernez, P. 2017. Atmospheric corrections and multi-conditional algorithm for multi-sensor remote sensing of suspended particulate matter in low-to-high turbidity levels coastal waters. *Remote Sensing*, 9(61)

ROESLER, C., AND E. BOSS. 2008. In situ measurement of the inherent optical properties (IOPs) and potential for harmful algal bloom detection and coastal ecosystem observations, p. 153–206. In M. Babin, C. Roesler, and J. Cullen [eds.], Realtime coastal observing systems for marine ecosystem dynamics and harmful algal blooms: Theory, instrumentation and modelling. UNESCO.

Shen, F., Verhoef, W., Zhou, Y., Salama, S. Liu, X. 2010. Satellite estimates of wide-range suspended sediment concentrations in Changjiang (Yangtze) estuary using MERIS data. *Estuaries and Coasts*, 33, pp.1420-1429

Vanhellemont, Q. and K. Ruddick. 2014. Turbid wakes associated with offshore wind turbines observed with Landsat 8. *Remote Sensing of Environment*, 145 : 105-115

Wang, L., Zhao, D., Yang, J., Chen, Y. 2012. Retrieval of total suspended matter from MODIS 250 m imagery in the Bohai Sea of China. *Journal of Oceanography*, Vol 68 (5) : 719-725

Zhou Wang, Alan Conrad Bovik, Hamid Rahim Sheikh and Eero P. Simoncelli, 2004. Image Quality Assessment: From Error Visibility to Structural Similarity. *IEEE TRANSACTIONS ON IMAGE PROCESSING*, VOL. 13, NO. 4,